

The 3.7 Å projection map of the glycerol facilitator GlpF: a variant of the aquaporin tetramer

Thomas Braun, Ansgar Philippsen¹, Sabine Wirtz, Mario J. Borgnia², Peter Agre², Werner Kühlbrandt³, Andreas Engel⁺ and Henning Stahlberg

M.E. Müller Institute for Microscopy and ¹Department of Structural Biology, Biozentrum, University of Basel, Klingelbergstrasse 70, CH-4056 Basel, Switzerland, ²Department of Biological Chemistry, Johns Hopkins University School of Medicine, Baltimore, MD 21205, USA and ³Max-Planck-Institute for Biophysics, Kennedyallee 70, D-60596 Frankfurt, Germany

Received February 21, 2000; revised May 5, 2000; accepted June 5, 2000

GlpF, the glycerol facilitator protein of *Escherichia coli*, is an archetypal member of the aquaporin superfamily. To assess its structure, recombinant histidine-tagged protein was over-expressed, solubilized in octylglucoside and purified to homogeneity. Negative stain electron microscopy of solubilized GlpF protein revealed a tetrameric structure of ~80 Å side length. Scanning transmission electron microscopy yielded a mass of 170 kDa, corroborating the tetrameric nature of GlpF. Reconstitution of GlpF in the presence of lipids produced highly ordered two-dimensional crystals, which diffracted electrons to 3.6 Å resolution. Cryoelectron microscopy provided a 3.7 Å projection map exhibiting a unit cell comprised of two tetramers. In projection, GlpF is similar to AQP1, the erythrocyte water channel. However, the major density minimum within each monomer is distinctly larger in GlpF than in AQP1.

INTRODUCTION

The glycerol uptake facilitator of *Escherichia coli* (GlpF; Boos *et al.*, 1990) is one of the few known diffusion facilitators in the inner membrane of this bacterium. Glycerol diffuses into the cell through GlpF and is phosphorylated by the glycerol kinase (GlpK), which prevents back-diffusion. Besides glycerol transport, the diffusion of polyols and urea derivatives through GlpF has been reported (Maurel *et al.*, 1994), but none of these substrates is transported in a phosphorylated state. In contrast, it remains unclear whether GlpF allows the passage of water.

GlpF is a member of the aquaporin protein superfamily (formerly known as the MIP family), which includes water channels (AQPs) and the facilitators of small solutes like glycerol (GLPs; Reizer *et al.*, 1993; Park and Saier, 1996; Heymann and

Engel, 1999). All of these channels are strictly selective for non-ionic compounds, thus preventing the dissipation of the membrane potential. Sequence comparisons have revealed an internal homology between the C- and N-terminal halves of all aquaporins, with highly conserved regions in the cytoplasmic loop B and the extracellular loop E (Heymann and Engel, 2000). According to the model of Jung *et al.* (1994), these two loops fold back into the membrane to form a channel akin to an hourglass. This region is believed to be the site of solute selectivity. Loop E of GlpF contains additional amino acids compared with AQP1. Other conserved residues have been found in the aquaporin superfamily by Froger *et al.* (1998) and were demonstrated by Lagree *et al.* (1999) to discriminate AQPs from GLPs. In addition, Heymann and Engel (2000) have identified a pair of residues that may determine the size of the pore. Tetrameric organization seems to be a general structural feature of aquaporins (Mitra *et al.*, 1995; Walz *et al.*, 1995; Li *et al.*, 1997; Hasler *et al.*, 1998; Daniels *et al.*, 1999; Ringler *et al.*, 1999). In contrast, analytical ultracentrifugation (Lagree *et al.*, 1998) and freeze fracture electron microscopy (Bron *et al.*, 1999) have indicated a monomeric organization for GlpF. Here we show by electron microscopy that purified GlpF solubilized in octyl-β-D-glucopyranoside (OG) is in fact a tetrameric particle that assembles into highly ordered arrays suitable for solving its structure by electron crystallography.

RESULTS

Protein expression and single particle analysis

GlpF carrying 10 C-terminal His residues was overexpressed in *E. coli*, solubilized and purified in OG as described by Borgnia

⁺Corresponding author. Tel: +41 61 267 2262; Fax: +41 61 267 2109; E-mail: Andreas.Engel@unibas.ch

T. Braun *et al.*

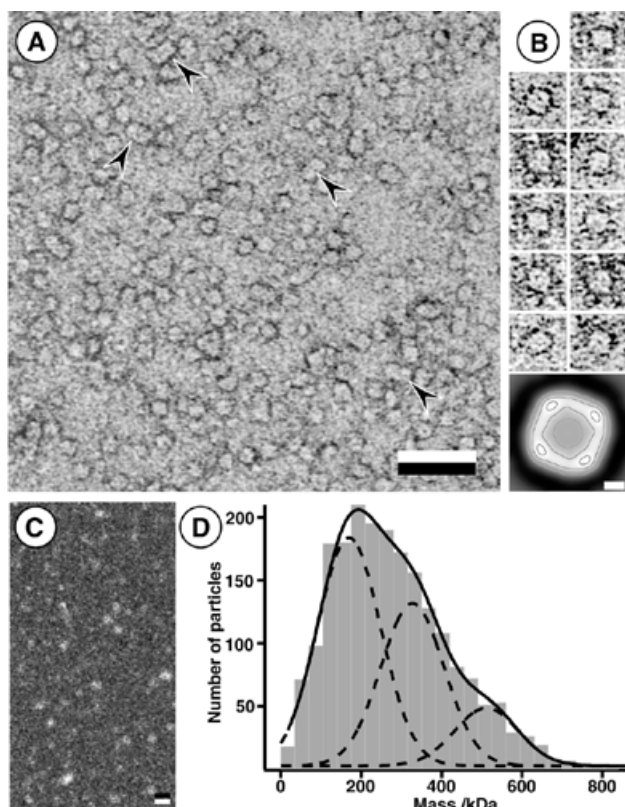


Fig. 1. TEM and STEM of solubilized GlpF. (A) Overview of negatively stained solubilized GlpF in TEM. Randomly oriented particles, often presenting a square shape, are predominant, but complexes of approximately twice the size are also seen (arrowheads). Scale bar corresponds to 450 Å. (B) Selected square-shaped particles. Image side length corresponds to 230 Å. Large inset: 4-fold symmetrized average after reference-free single particle analysis. Scale bar corresponds to 20 Å. (C) Dark-field STEM image of freeze-dried solubilized GlpF recorded at 3.3 e/Å². Scale bar corresponds to 100 Å. (D) Result of STEM mass measurements. The mass histogram comprising 2073 measurements was fitted with two significant Gauss peaks at 170 kDa (total error of ± 12 kDa) and 327 ± 20 kDa, respectively, and a minor peak at 511 ± 31 kDa.

et al. (1999). Analysis of purified and solubilized GlpF by SDS-PAGE revealed a prominent band at an apparent mol. wt of 30 kDa. GlpF purified in this way is functionally active (M.J. Borgnia, personal communication). Transmission electron microscopy (TEM) of negatively stained solubilized GlpF revealed two different particle populations (Figure 1A): smaller, often square-shaped particles and larger complexes of about twice the size of the small ones (arrowheads). Tilting of the tetramers possibly related to the His tag (Ringler *et al.*, 1999) may explain the heterogeneous appearance of the small particles. Nevertheless, 1294 single particles were selected automatically (Figure 1B), windowed and subjected to reference-free alignment (Penczek *et al.*, 1992). The resulting square-shaped average projection had a side length of ~80 Å and four weak peripheral densities (Figure 1B, large inset).

Purified GlpF particles were also freeze-dried and imaged with a scanning transmission electron microscope (STEM) for mass measurements (Müller and Engel, 1998). The low-dose

dark-field image in Figure 1C shows particles of different brightness and size, whose masses were calculated and sorted in a histogram after mass loss correction (Figure 1D; Müller *et al.*, 1992). The mass histogram resulting from the analysis of 100 images (2073 particles in total) exhibits a broad asymmetric distribution with a single maximum at ~190 kDa. Two independent Marquardt algorithms (see Methods) produced a three-peak fit with Gauss profiles having a standard deviation of 111 kDa located at 170, 327 and 511 kDa. The experimental errors for these three peaks were estimated as 12, 20 and 31 kDa, respectively, taking the standard deviation, the number of particles within a peak and the calibration accuracy into account. A size of 170 kDa is compatible with a GlpF tetramer including the four His tags and their spacers (12 kDa), plus 60 kDa of OG accounting for two micelles (Walz *et al.*, 1994). Thus, 327 kDa corresponds to an octamer and 511 kDa to a dodecamer. The abundance of tetrameric particles documented by the mass histogram is consistent with the results from negatively stained preparations (Figure 1A).

Two-dimensional crystallization

Solubilized GlpF was reproducibly crystallized using a continuous flow dialysing device (Jap *et al.*, 1992) as described in Methods. Analysis in the TEM showed polycrystalline vesicles with diameters up to 40 µm and mostly monocrystalline double-layered sheets with rectangular shapes and diameters up to 8 µm (Figure 2A). Some tubular structures were seen in many reconstitution experiments. However, their crystallinity was far inferior to that of the double-layered sheets. The crystal quality of the latter was assessed by electron diffraction of frozen-hydrated samples. The diffraction pattern recorded with a 1k × 1k CCD camera shows spots beyond 3.6 Å (Figure 2B) but weak structure factors between 7 and 5 Å. The four (28,7) orders marked by arrowheads correspond to a resolution of 3.6 Å. Since the two layers were rotated with respect to each other, two lattices are indicated.

Electron microscopy and image treatment

Images of negatively stained crystals were recorded in a TEM and analysed by correlation averaging (Baumeister *et al.*, 1982). The unit cell containing two tetrameric structures exhibited a *P4* symmetry. Adjacent tetramers were differently stained similar to AQP1 crystals (Walz *et al.*, 1994), indicating their up-down orientation (data not shown).

Images of frozen-hydrated crystals recorded at low dose revealed sharp spots when examined by optical diffraction out to a resolution of 7 Å. The eight best images were digitized and processed by the MRC program package (Henderson *et al.*, 1986, 1990). The unit cell size was determined to 104 Å. The phase residuals of the merged data obtained after lattice unbending and transfer function correction indicated significant information up to a resolution of 3.7 Å (Table I), yielding the projection map shown in Figure 3. In contrast to AQP1 crystals with *P42₂* symmetry, the GlpF crystals exhibit a *P4* symmetry (Table II), since oppositely oriented tetramers are rotated about their 4-fold axes by different amounts. Thus, the striking similarity of the two oppositely handed tetramers shown in Figure 3 demonstrates the quality of the map.

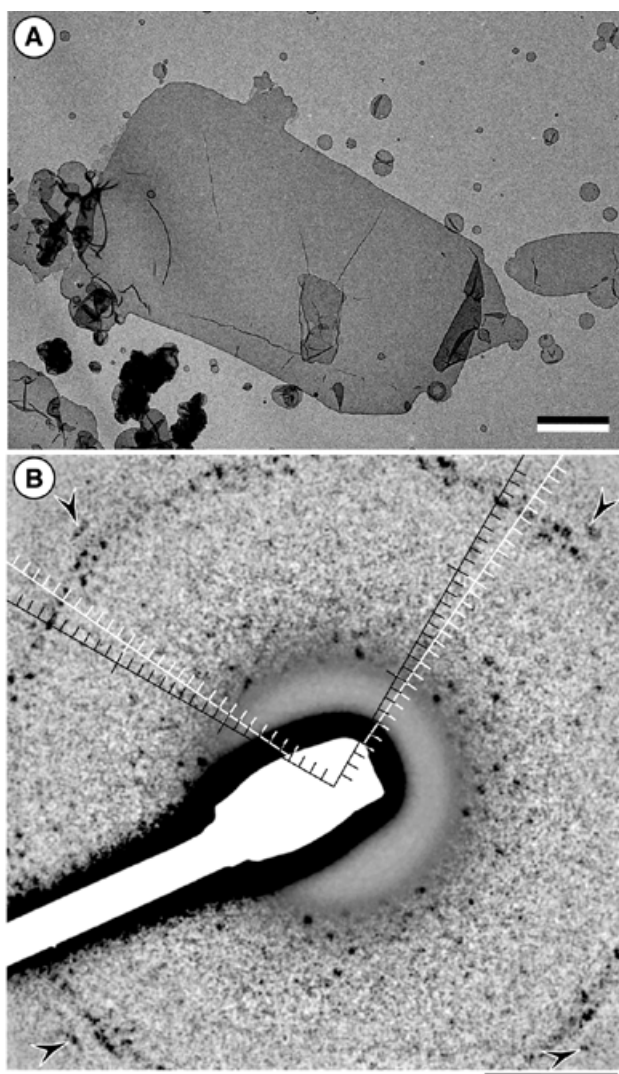


Fig. 2. Two-dimensional (2D) crystal of GlpF reconstituted in the presence of lipid. **(A)** The rectangular double-layered crystals were usually mono-crystalline and well ordered and had sizes of several micrometres in diameter. Scale bar corresponds to 2 μm . **(B)** The electron diffraction pattern of a frozen-hydrated 2D crystal demonstrates the excellent crystallinity of such rectangular crystals. Two different lattices of the double-layered crystal are overlaid. Two hair crosses indicate the superimposed lattices. Diffraction orders marked by arrowheads correspond to a resolution of 3.6 \AA . The scale bar represents $1/10 \text{\AA}^{-1}$.

DISCUSSION

Here we present the first structural analysis of GlpF, the archetypal member of the GlpF subcluster of the aquaporin superfamily (Heymann and Engel, 1999). Negative stain electron microscopy and mass measurements of freeze-dried unstained preparations in the STEM demonstrate that OG-solubilized GlpF exhibits the same tetrameric structure as other aquaporins studied previously: AQP1 (Smith and Agre, 1991; Walz *et al.*, 1994), AqpZ (Ringler *et al.*, 1999), MIP (Hasler *et al.*, 1998) and TIP (Daniels *et al.*, 1999). This result is in contrast with reports of monomeric GlpF and the hypothesis that glycerol facilitators are

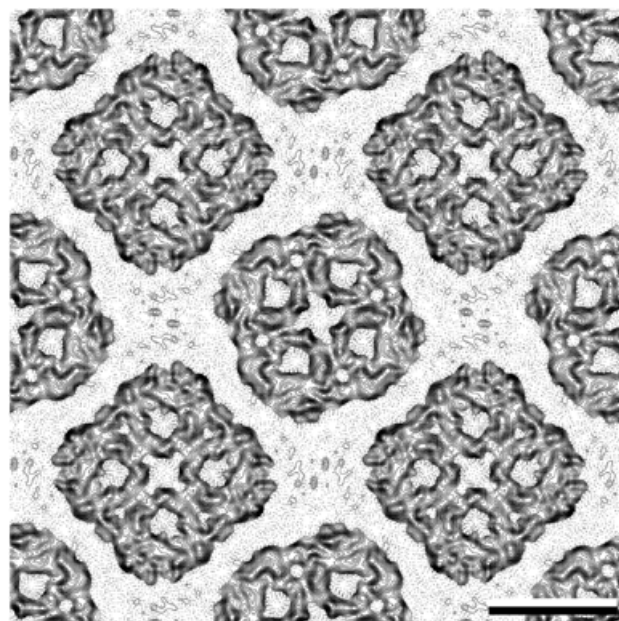


Fig. 3. The $P4$ -symmetrized 3.7 \AA projection structure of GlpF. The map was calculated by merging eight electron micrographs after unbending crystal distortions and correcting the transfer function. The phase residuals indicated significant information up to 3.7 \AA resolution (see Table I). A negative temperature factor of -20\AA^2 was applied. Scale bar corresponds to 50 \AA .

monomeric whereas water channels require tetramerization (Lagree *et al.*, 1998; Bron *et al.*, 1999). However, the apparent tetrameric nature of GlpF reported here is consistent with the model proposed by Voegelé *et al.* (1993) in which GlpF interacts with the tetrameric glycerol kinase GlpF to stimulate glycerol phosphorylation.

In our hands, GlpF crystallized under similar conditions to AQP1 (Walz *et al.*, 1995), but at pH 8.5 instead of pH 6 and at much lower MgCl_2 concentration. The $P4$ unit cell houses eight GlpF monomers, has a side length of 104 \AA and is thus 8% larger than the $P4_21_2$ unit cell of AQP1 (96 \AA ; Walz *et al.*, 1994). Electron diffraction experiments, yielding diffraction maxima to 3.6 \AA , document the crystalline quality of these double-layered sheets and suggest their suitability for structure determination at atomic resolution. This is further supported by the 3.7 \AA projection map obtained by processing images of frozen-hydrated crystals recorded at liquid helium temperature.

It is interesting to compare the first high-resolution projection structure of the archetypal member of the GLP subcluster with that of AQP1, the first aquaporin structurally analysed to high resolution (Figure 4; Cheng *et al.*, 1997; Li *et al.*, 1997; Walz *et al.*, 1997; Mitsuoka *et al.*, 1999). The density maxima marked in the AQP1 map (Figure 4B) appear to be slightly shifted and of different amplitude to the maxima in the GlpF map (Figure 4A). They are related to six tilted helices that surround a central structure produced by loops B and E (Mitsuoka *et al.*, 1999). According to the hourglass model (Jung *et al.*, 1994), these loops are close to the channel (marked by an X in Figure 4). Thus, differences between GlpF and AQP1 in this region are of particular interest. While the projection map of AQP1 shows a weak

Table I. Phase residuals in resolution ranges (random = 90°) and crystallographic data

Resolution (Å)		IQ value (signal/noise ≈ 8/IQ) ^a							IQ-weighted residuals
From	To	1	2	3	4	5	6	7	
200.0	9.9	5.7	14.8	23.0	37.7	41.0	48.5	47.6	14.4
		299	324	212	123	109	74	44	1185
9.8	7.0	7.6	10.1	17.2	24.0	40.5	47.7	44.6	24.3
		17	64	143	161	131	120	70	706
7.0	5.7	0.0	31.9	18.2	30.9	37.0	47.4	59.1	39.1
		0	1	25	70	128	97	84	405
5.7	4.9	0.0	40.4	32.3	32.0	47.3	47.6	66.9	47.7
		0	1	17	40	92	86	93	329
4.9	4.4	0.0	0.0	22.4	33.6	50.7	62.6	63.5	50.4
		0	0	13	49	92	86	80	320
4.4	4.0	0.0	0.0	47.5	55.9	57.3	69.0	64.6	60.9
		0	0	15	45	71	97	81	309
4.0	3.7	0.0	0.0	62.8	41.8	57.0	62.3	55.7	55.9
		0	0	3	38	86	105	84	316
3.7	3.5	0.0	0.0	26.3	62.1	77.2	79.4	82.6	74.0
		0	0	8	27	63	80	79	257
3.5	3.3	0.0	0.0	59.8	87.8	75.2	91.4	79.9	82.0
		0	0	6	27	65	73	70	241
Plane group symmetry				P4					
Lattice constants				a = b = 104 Å					
Number of images				8					
Resolution limit for merging				3.7 Å (Figure 3), 4.0 Å (Figure 4)					

^aSpots are classified according to Henderson *et al.* (1986). Phase residuals (in degrees, top line) during merging and the number of spots (bottom line) in each class are given for different resolution ranges.

density at this position, GlpF seems to have a much larger hole with no inner structure discernible in the projection map.

The striking similarity of the GlpF tetramers of opposing handedness in Figure 3 suggests that their 4-fold axes were parallel to the optical axis of the microscope, similar to the situation of the AQP1 crystals. Hence, tilting of tetramers can be excluded as a major reason for the differences observed. Another possibility could be that the pore of GlpF is parallel to the 4-fold axis of the tetramer, whereas the AQP1 channel is tilted. Nevertheless, it is more compelling to speculate that the apparently larger pore is required for the diffusion of glycerol and other small anionic solutes (Maurel *et al.*, 1994). How such a pore prevents the passage of protons and other ions is a mystery still to be enlightened. The highly ordered two-dimensional crystals presented here are a first essential step towards this goal.

METHODS

Protein expression. A construct of GlpF with a His₁₀ tag at the N-terminus was overexpressed in *E. coli*, solubilized in OG and isolated by Ni-chelation chromatography (Borgnia *et al.*, 1999;

Ringler *et al.*, 1999). The solubilized protein was stable in 3% OG at 4°C for weeks and could be concentrated by centrifugation to 12 mg/ml without precipitation.

Crystallization. The GlpF was dialysed in a continuous flow dialysis machine (Jap *et al.*, 1992) against a buffer containing 10 mM tricine pH 8.5, 5 mM MgCl₂, 100 mM NaCl, 10 mM dithiothreitol and *E. coli* lipid (Avanti Polar lipids, Inc., USA) with a lipid to protein ratio (LPR) ranging from 0.6 to 1.4 (w/w) using the following temperature profile: 25°C for 12 h, a linear increase to 40°C over the next 12 h, 40°C for 24 h and a linear decrease to 25°C over 6 h. Protein concentrations between 1 and 3 mg/ml were used.

STEM mass determination. Purified GlpF (50 µg/ml) was adsorbed to thin carbon films, washed extensively with quartz distilled water, freeze-dried, and imaged with a Vacuum Generators HB5 STEM at doses of ~3.3 e/Å² (Müller and Engel, 1998). The IMPSYS software package was used to extract mass values of all particles discernible on the dark-field images. These values were corrected for the experimentally measured dose-associated mass loss (Müller *et al.*, 1992), distributed in a histogram and approximated by Gaussian curve fitting with a Marquardt algorithm (Bevington, 1969). The mass values were

Table II. Internal phase residuals of one image according to the plane group symmetry

Plane group	Phase residual (degrees) versus other spots (90° = random)		Phase residual (degrees) versus theoretical of 0° or 180° (45° = random)		Target residual (degrees)
P1	7.1	(544)	5.0	(544)	
P2	46.3	(272)*	23.2	(544)	48.9
P12_b	59.4	(120)	14.5	(20)	34.1
P12_a	57.5	(119)	11.6	(18)	34.0
P121_b	67.8	(120)	14.2	(20)	34.1
P121_a	73.9	(119)	46.7	(18)	34.0
C12_b	59.4	(120)	14.5	(20)	34.1
C12_a	57.5	(119)	11.6	(18)	34.0
P222	52.0	(511)	23.2	(544)	41.4
P2221b	64.2	(511)	23.3	(544)	41.4
P2221a	57.3	(511)	23.3	(544)	41.4
P22121	61.9	(511)	23.2	(544)	41.4
C222	52.0	(511)	23.2	(544)	41.4
P4	34.2	(568)*	23.2	(544)	40.5
P422	45.2	(1046)	23.2	(544)	37.0
P4212	56.8	(1046)	23.4	(544)	37.0

Internal phase residuals determined using the program ALLSPACE (Valpuesta *et al.*, 1994) for reflections to 3.7 Å resolution with IQ values of 1–5. Only plane groups compatible with the GlpF lattice are shown. The numbers of comparisons are shown in parentheses. An asterisk indicates the symmetry that yields a residual better than the target residual.

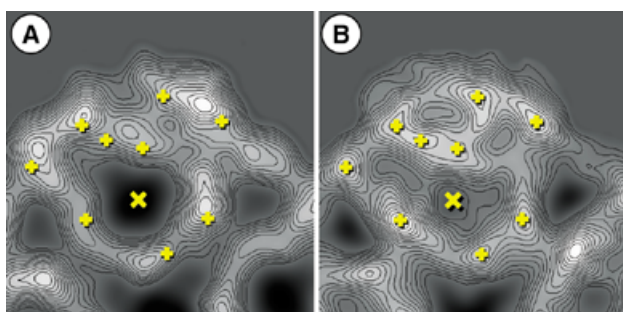


Fig. 4. Comparison of GlpF and AQP1 at 4 Å resolution. **(A)** GlpF monomer. **(B)** AQP1 monomer. Overlaid crosses mark the position of density maxima found in AQP1. The depression in the AQP1 monomer, thought to represent the pore, is marked by an X. The most prominent difference revealed by the GlpF monomer is the central depression of ~10 Å diameter, which is significantly larger than the one in AQP1 that exhibits a complex shape. Further differences are seen in the surrounding density maxima. They correspond to the projection of overlapping highly tilted helices. The minima around the 4-fold axes and between the monomers are rather similar. The image side length corresponds to 41 Å.

also analysed using a commercial program (Igor pro, www.wavemetrics.com) for Histogram calculations and Gauss peak fitting by a Levenberg–Marquardt algorithm. The total experimental error was calculated as the standard error of the mean, plus 5% of the measured particle mass to account for the absolute calibration uncertainty.

Transmission electron microscopy. For single particle analysis, the protein (50 µg/ml) sample was absorbed for 5 s onto glow discharged carbon film-coated copper grids, washed three times in distilled water for 5 s and stained with 0.75% uranyl formate. Images were recorded under low-dose conditions with a Hitachi H-8000 TEM at 200 kV and nominal magnification of 50 000× on Kodak SO-163 films.

For cryoelectron microscopy, grids were prepared by the back-injection technique (Hirai *et al.*, 1999) with 1% trehalose, quickly frozen in liquid ethane and transferred with a Gatan 626 cryo holder into a Hitachi H-8000 TEM. Images were recorded at 90 K at 200 kV and 50 000× nominal magnification on Kodak SO-163 film, using a homemade spot-scan and low-dose set-up programmed on the Tietz CCD remote control system (Tietz Video & Imaging Processing System, Gauting, Germany). The dose per negative was 5 e/Å². Electron diffraction patterns of vitrified crystals were acquired by the 1k × 1k Tietz CCD camera. Alternatively, images were recorded with a JEOL 3000SFF (MPI for Biophysics, Frankfurt) in spot-scan mode and operated at 300 kV, 4.2 K and 70 000× nominal magnification. The dose for recording an image was 17 e/Å².

Image processing. Micrographs of negatively stained samples were digitized using a Leafscan-45 scanner (Leaf Systems, Inc., Westborough, MA) at 4 Å/pixel at the specimen level. Single particles were picked automatically, windowed, aligned with a reference-free alignment procedure (Penczek *et al.*, 1992; www.wadsworth.org/spider_doc/spider/docs/refreealign.html) and classified using the SPIDER software (Frank *et al.*, 1996).

T. Braun et al.

Cryo-TEM negatives of two-dimensional crystals were digitized using a Zeiss Phodis scanner (Carl Zeiss, Oberkochen, Germany) at 1 Å/pixel on the specimen level. Image processing was performed with the MRC software package (Henderson *et al.*, 1986, 1990). In a first run, images were unbent three times using the Fourier-filtered images themselves as a reference. The merged amplitudes and phases from eight images were then used with the program MAKETRAN to create two synthetic references, applying two different negative temperature factors. All images were now unbent using the reference with the smaller negative temperature factor. The unbent images were then refined by unbending them a second time, using the reference with the stronger negative temperature factor, this time allowing only very small (5 pixels/unit-cell) displacements of the units-cells.

To compare the GlpF and AQP1 monomers, the SEMPER software was used. First, the non-crystalline symmetry in the GlpF crystals was applied (mirroring and rotational alignment of the two adjacent tetramers) to approach the $P4_212$ symmetry used for AQP1. The monomers of GlpF and AQP1 were then interpolated to the same scale, aligned translationally and rotationally, and displayed with identical grey value level ranges and contours to aid comparison.

ACKNOWLEDGEMENTS

We thank Deryck Mills for the introduction and expert support with the Jeol 3000SFF microscope and Vinzenz Unger for advice on the use of the MAKETRAN routine. We are indebted to Yoshinori Fujiyoshi, Kaoru Mitsuoka and Thomas Walz for providing the AQP1 data, and Lorenz Hasler and Shirley Müller for their expert help. The work was supported by the Swiss National Foundation for Scientific Research (NF grant No. 4036-44062 to A.E.), the M.E. Müller Foundation of Switzerland and the National Institutes of Health (to P.A.).

REFERENCES

- Baumeister, W., Karrenberg, F., Rachel, R., Engel, A., ten Heggeler, B. and Saxton, W.O. (1982) The major cell envelope protein of *Micrococcus radiodurans* (R1). Structural and chemical characterization. *Eur. J. Biochem.*, **125**, 535–544.
- Bevington, P.R. (1969) *Data Reduction and Error Analysis for the Physical Sciences*. McGraw-Hill, New York, NY.
- Boos, W., Ehmann, U., Forkl, H., Klein, W., Rimmele, M. and Postma, P. (1990) Trehalose transport and metabolism in *Escherichia coli*. *J. Bacteriol.*, **172**, 3450–3461.
- Borgnia, M.J., Kozono, D., Calamita, G., Maloney, P.C. and Agre, P. (1999) Functional reconstitution and characterization of AqpZ, the *E. coli* water channel protein. *J. Mol. Biol.*, **291**, 1169–1179.
- Bron, P. *et al.* (1999) Oligomerization state of MIP proteins expressed in *Xenopus* oocytes as revealed by freeze-fracture electron-microscopy analysis. *J. Struct. Biol.*, **128**, 287–296.
- Cheng, A., van Hoek, A.N., Yeager, M., Verkman, A.S. and Mitra, A.K. (1997) Three-dimensional organization of a human water channel. *Nature*, **387**, 627–630.
- Daniels, M.J., Chrispeels, M.J. and Yeager, M. (1999) Projection structure of a plant vacuole membrane aquaporin by electron cryo-crystallography. *J. Mol. Biol.*, **294**, 1337–1349.
- Frank, J., Radermacher, M., Penczek, P., Zhu, J., Li, Y., Ladjadj, M. and Leith, A. (1996) SPIDER and WEB: Processing and visualization of images in 3D electron microscopy and related fields. *J. Struct. Biol.*, **116**, 190–199.
- Froger, A., Tallur, B., Thomas, D. and Delamarche, C. (1998) Prediction of functional residues in water channels and related proteins. *Protein Sci.*, **7**, 1458–1468.
- Hasler, L., Walz, T., Tittmann, P., Gross, H., Kistler, J. and Engel, A. (1998) Purified lens major intrinsic protein (MIP) forms highly ordered tetragonal two-dimensional arrays by reconstitution. *J. Mol. Biol.*, **279**, 855–864.
- Henderson, R., Baldwin, J.M., Downing, K.H., Lepault, J. and Zemlin, F. (1986) Structure of purple membrane from *Halobacterium halobium*: recording, measurement and evaluation of electron micrographs at 3.5 Å resolution. *Ultramicroscopy*, **19**, 147–178.
- Henderson, R., Baldwin, J.M., Ceska, T.A., Zemlin, F., Beckmann, E. and Downing, K.H. (1990) Model for the structure of bacteriorhodopsin based on high-resolution electron cryo-microscopy. *J. Mol. Biol.*, **213**, 899–929.
- Heymann, J.B. and Engel, A. (1999) Aquaporins: Phylogeny, structure, and physiology of water channels. *News Physiol. Sci.*, **14**, 187–193.
- Heymann, B. and Engel, A. (2000) Structural clues in the sequences of the aquaporins. *J. Mol. Biol.*, **295**, 1039–1053.
- Hirai, T., Murata, K., Kimura, Y. and Fujiyoshi, Y. (1999) Trehalose embedding technique for high-resolution electron crystallography: application to structural study on bacteriorhodopsin. *J. Electron Microsc.*, **48**, 653–685.
- Jap, B.K., Zulauf, M., Scheybani, T., Hefti, A., Baumeister, W., Aebi, U. and Engel, A. (1992) 2D crystallization: from art to science. *Ultramicroscopy*, **46**, 45–84.
- Jung, J.S., Preston, G.M., Smith, B.L., Guggino, W.B. and Agre, P. (1994) Molecular structure of the water channel through aquaporin CHIP. The hourglass model. *J. Biol. Chem.*, **269**, 14648–14654.
- Lagree, V., Froger, A., Deschamps, S., Pellerin, I., Delamarche, C., Bonnet, G., Gouranton, J., Thomas, D. and Hubert, J.F. (1998) Oligomerization state of water channels and glycerol facilitators. Involvement of loop E. *J. Biol. Chem.*, **273**, 33949–33953.
- Lagree, V., Froger, A., Deschamps, S., Hubert, J.F., Delamarche, C., Bonnet, G., Thomas, D., Gouranton, J. and Pellerin, I. (1999) Switch from an aquaporin to a glycerol channel by two amino acids substitution. *J. Biol. Chem.*, **274**, 6817–6819.
- Li, H., Lee, S. and Jap, B.K. (1997) Molecular design of aquaporin-1 water channel as revealed by electron crystallography. *Nature Struct. Biol.*, **4**, 263–265.
- Maurel, C., Reizer, J., Schroeder, J.I., Chrispeels, M.J. and Saier, M.H., Jr (1994) Functional characterization of the *Escherichia coli* glycerol facilitator, GlpF, in *Xenopus* oocytes. *J. Biol. Chem.*, **269**, 11869–11872.
- Mitra, A.K., van Hoek, A.N., Wiener, M.C., Verkman, A.S. and Yeager, M. (1995) The CHIP28 water channel visualized in ice by electron crystallography. *Nature Struct. Biol.*, **2**, 726–729.
- Mitsuoka, K., Murata, K., Walz, T., Hirai, T., Agre, P., Heymann, J.B., Engel, A. and Fujiyoshi, Y. (1999) The structure of aquaporin-1 at 4.5-Å resolution reveals short α -helices in the center of the monomer. *J. Struct. Biol.*, **128**, 34–43.
- Müller, S., Goldie, K.N., Bürki, R., Häring, R. and Engel, A. (1992) Factors influencing the precision of quantitative scanning transmission electron microscopy. *Ultramicroscopy*, **46**, 317–334.
- Müller, S.A. and Engel, A. (1998) Mass measurement in the scanning transmission electron microscope: A powerful tool for studying membrane proteins. *J. Struct. Biol.*, **121**, 219–230.
- Park, J.H. and Saier, M.H., Jr (1996) Phylogenetic characterization of the MIP family of transmembrane channel proteins. *J. Membr. Biol.*, **153**, 171–180.
- Penczek, P., Radermacher, M. and Frank, J. (1992) Three-dimensional reconstruction of single particles embedded in ice. *Ultramicroscopy*, **40**, 33–53.
- Reizer, J., Reizer, A. and Saier, M.H., Jr (1993) The MIP family of integral membrane channel proteins: sequence comparisons, evolutionary relationships, reconstructed pathway of evolution, and proposed functional differentiation of the two repeated halves of the proteins. *Crit. Rev. Biochem. Mol. Biol.*, **28**, 235–257.

- Ringler, P., Borgnia, M.J., Stahlberg, H., Maloney, P.C., Agre, P. and Engel, A. (1999) Structure of the water channel AqpZ from *Escherichia coli* revealed by electron crystallography. *J. Mol. Biol.*, **291**, 1181–1190.
- Smith, B.L. and Agre, P. (1991) Erythrocyte Mr 28,000 transmembrane protein exists as a multisubunit oligomer similar to channel proteins. *J. Biol. Chem.*, **266**, 6407–6415.
- Valpuesta, J.M., Carrascosa, J.L. and Henderson, R. (1994) Analysis of electron microscope images and electron diffraction patterns of thin crystals of ϕ 29 connectors in ice. *J. Mol. Biol.*, **240**, 281–287.
- Voegelé, R.T., Sweet, G.D. and Boos, W. (1993) Glycerol kinase of *Escherichia coli* is activated by interaction with the glycerol facilitator. *J. Bacteriol.*, **175**, 1087–1094.
- Walz, T., Smith, B.L., Agre, P. and Engel, A. (1994) The three-dimensional structure of human erythrocyte aquaporin CHIP. *EMBO J.*, **13**, 2985–2993.
- Walz, T., Typke, D., Smith, B.L., Agre, P. and Engel, A. (1995) Projection map of aquaporin-1 determined by electron crystallography. *Nature Struct. Biol.*, **2**, 730–732.
- Walz, T., Hirai, T., Murata, K., Heymann, J.B., Mitsuoka, K., Fujiyoshi, Y., Smith, B.L., Agre, P. and Engel, A. (1997) The three-dimensional structure of aquaporin-1. *Nature*, **387**, 624–627.

DOI: 10.1093/embo-reports/kvd022